Journal of Sound and Vibration (1999) **219**(1), 175–188
Article No. jsvi.1998.1852, available online at http://www.idealibrary.com.on IDEAL

LETTERS TO THE EDITOR

VIBRATION CONTROL OF A ROTOR SYSTEM BY DISK TYPE ELECTRORHEOLOGICAL DAMPER

G. Z. Yao and Y. Qiu

State Key Laboratory of Mechanical Structural Strength and Vibration, Xi'an Jiao Tong University, Xi'an 710049, *Shananxi, P.R.C.*

and

G. Meng* and T. Fang

Institute of Vibration Engineering, Northwestern Polytechnical University, Xi'an 710072, *Shaanxi, P.R.C.*

and

Y. B. Fan

Foshan University, Foshan 528000, *Guangdong, P.R.C.*

(*Received* 3 *September* 1997, *and in final form* 22 *June* 1998)

1. INTRODUCTION

Electrorheological (ER) fluid is a kind of smart material which has the merits of fast response, easy control and low energy consumption. It has a broad application to vibration control. Since Winslow [1] first reported the ER effect in 1947, many achievements have been obtained in vibration control [2–5]. The application of ER fluid to the vibration control of rotor systems was first proposed by Nikolajsen and Hoque [3]. Through experiments they demonstrated the capability of the application of ER fluid in rotor systems. The resonant vibration around the first critical speed was suppressed by the ER damper. In this paper, a new disk type ER damper is designed and its application to the vibration suppression of a rotor system is investigated theoretically and experimentally. Both the suppression of the resonant vibration around the first critical speed and the suppression of the large response caused by the sudden unbalance are considered.

2. STRUCTURE OF ER DAMPER AND EXPERIMENTAL ARRANGEMENT

The new designed ER damper consists of a moving part with 4 disks and a stationary part with 5 disks. The disks are placed uniformly and alternatively with a uniform gap of 1·7 mm. For clarity, only a part of them is shown in Figure 1. The stationary part is connected to the negative pole of the electric field, while the moving part to the positive one.

The experimental rig is composed of a shaft, a disk D, an ER damper, and a motor, as shown in Figure 2. The shaft is 9·5 mm in diameter and 500 mm in length. The moving part of the ER damper, together with the outer ring of the bearing B, is mounted on a squirrel cage. Both of them move in the same way. The shaft is driven by a d.c. motor, the speed of which may be adjusted continually from 0 to 12 000 rpm.

*Now at Foshan University, Foshan 528000, Guangdon, P.R.C.

0022–460X/99/010175 + 14 $30.00/0

3. ANALYSIS MODEL

The mathematical model of the simplified experimental rig is shown in Figure 3. The left support is assumed as a stiff support. A coordinate system is established as shown in Figure 3. According to the analysis method of rotordynamics [6], the governing equations can be obtained as:

$$\begin{cases} m_D\ddot{x}_D + c_D\dot{x}_D + k_{rr}\left[x_D - \left(1+\dfrac{a}{l}\right)x_B\right] + k_{\varphi r}\alpha = m_1 e\omega^2\cos\omega t \\ m_D\ddot{y}_D + c_D\dot{y}_D + k_{rr}\left[y_D - \left(1+\dfrac{a}{l}\right)y_B\right] + k_{\varphi r}\beta = m_1 e\omega^2\sin\omega t \\ I_d\ddot{\alpha} + I_P\omega\dot{\beta} + k_{\varphi r}x_D + k_{\varphi\varphi}\alpha = 0 \\ I_d\ddot{\beta} - I_P\omega\dot{\alpha} + k_{\varphi r}y_D + k_{\varphi\varphi}\beta = 0 \\ m_B\ddot{x}_B + k_{rr}\left[\left(1+\dfrac{a}{l}\right)x_B - x_D\right] + k_s x_B + c_B\dot{x}_B + c_{ER}\dot{x}_B = F_{ERx} \\ m_B\ddot{y}_B + k_{rr}\left[\left(1+\dfrac{a}{l}\right)y_B - y_D\right] + k_s y_B + c_B\dot{y}_B + c_{ER}\dot{y}_B = F_{ERy} \end{cases} \tag{1}$$

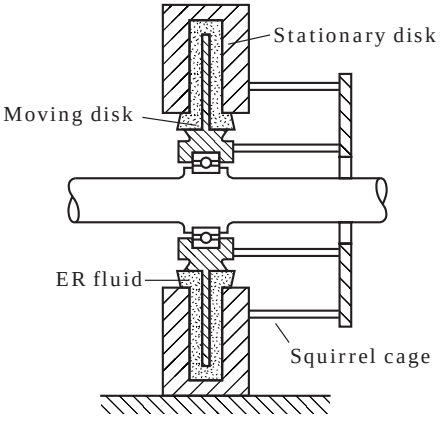

Figure 1. Cross section of ER damper.

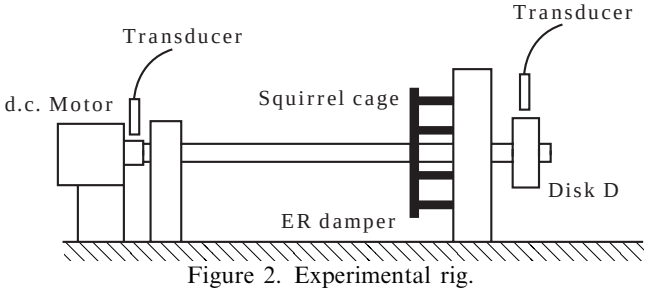

Figure 2. Experimental rig.

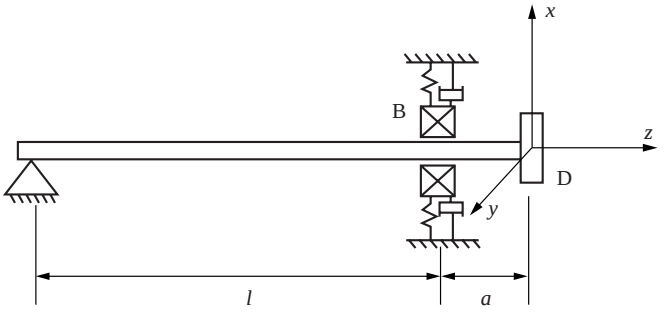

Figure 3. Simplified mathematical model.

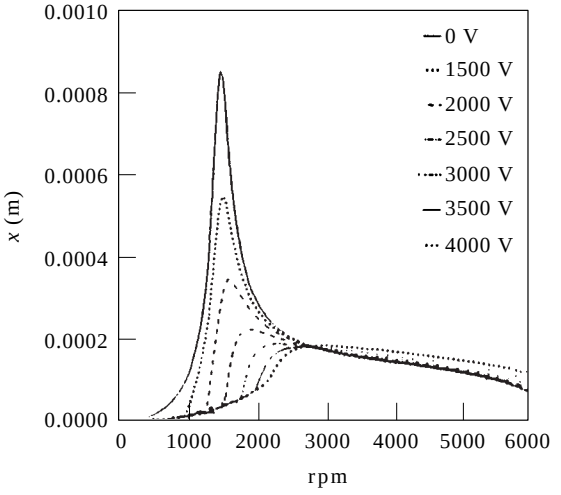

Figure 4. Response curve of B.

where m_D and m_B are masses of the disk and bearing B respectively; c_D and c_B are external damping coefficients; m_1 is the unbalanced mass of disk D; e is the eccentricity; ω is the rotational speed of the shaft; I_d and I_p are diameter moment-of-inertia and polar moment-of-inertia; c_{ER}, F_{ERx} and F_{ERy} are damping coefficient and friction forces in the x and y directions of the ER damper respectively. α and β are two Euler angles [6]. k_{rr}, $k_{\varphi\varphi}$, $k_{r\varphi}(=k_{\varphi r})$ can be obtained as

$$\begin{bmatrix} k_{rr} & k_{r\varphi} \\ k_{\varphi r} & k_{\varphi\varphi} \end{bmatrix} = \frac{A_4}{A_5} \begin{bmatrix} A_2 & -A_3 \\ -A_3 & A_1 \end{bmatrix} \tag{2}$$

in which

$$A_1 = 2k_s l^2(l+a) + 6EI(l+a)^2, \qquad A_2 = 6EI + 2k_s l^2(l+3a)$$

$$A_3 = 6EI(l+a) + ak_s l^2(2l+3a), \qquad A_4 = 6EIk_s l^2, \qquad A_5 = A_1 \times A_2 - A_3^2$$

where E is the elastic modulus of the shaft, I is the moment-of-inertia and k_s is the stiffness of the squirrel cage

$$k_s = \frac{12nE_s\pi d^4}{64h^3}$$

where n is the number of the squirrel cage bars, E_s is the elastic modulus of the bars, d is the diameter of the bars and h is the support length of the bars.

Let $\mathbf{u} = [x_D \;\; y_D \;\; \alpha \;\; \beta \;\; x_B \;\; y_B]^{\mathrm{T}}$, and equation (1) can be written as

$$\mathbf{M\ddot{u}} + \mathbf{C\dot{u}} + \mathbf{Ku} = \mathbf{F} \tag{3}$$

where

$$\mathbf{M} = \begin{bmatrix} m_D & 0 & 0 & 0 & 0 & 0 \\ 0 & m_D & 0 & 0 & 0 & 0 \\ 0 & 0 & I_d & 0 & 0 & 0 \\ 0 & 0 & 0 & I_d & 0 & 0 \\ 0 & 0 & 0 & 0 & m_B & 0 \\ 0 & 0 & 0 & 0 & 0 & m_B \end{bmatrix}$$

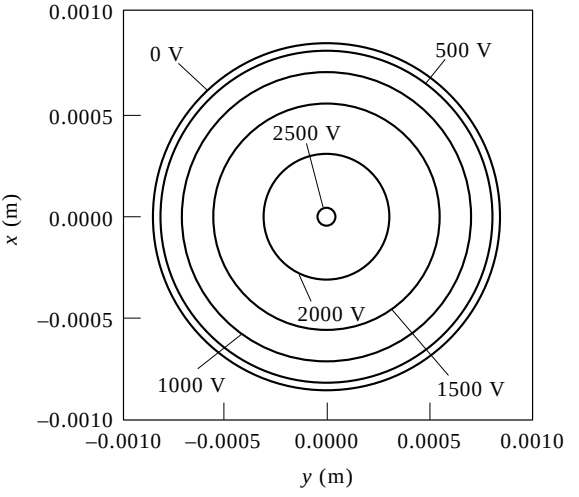

Figure 5. Critical orbits of B.

$$\mathbf{C} = \begin{bmatrix} c_D & 0 & 0 & 0 & 0 & 0 \\ 0 & c_D & 0 & 0 & 0 & 0 \\ 0 & 0 & 0 & I_p\omega & 0 & 0 \\ 0 & 0 & -I_p\omega & 0 & 0 & 0 \\ 0 & 0 & 0 & 0 & c_B + c_{ER} & 0 \\ 0 & 0 & 0 & 0 & 0 & c_B + c_{ER} \end{bmatrix}$$

$$\mathbf{K} = \begin{bmatrix} k_{rr} & 0 & k_{\varphi r} & 0 & -\left(1 + \frac{a}{l}\right)k_{rr} & 0 \\ 0 & k_{rr} & 0 & k_{\varphi r} & 0 & -\left(1 + \frac{a}{l}\right)k_{rr} \\ k_{\varphi r} & 0 & k_{\varphi\varphi} & 0 & 0 & 0 \\ 0 & k_{\varphi r} & 0 & k_{\varphi\varphi} & 0 & 0 \\ -k_{rr} & 0 & 0 & 0 & k_{rr}\left(1 + \frac{a}{l}\right) + k_s & 0 \\ 0 & -k_{rr} & 0 & 0 & 0 & k_{rr}\left(1 + \frac{a}{l}\right) + k_s \end{bmatrix}$$

$$\mathbf{F} = [m_1 e\omega^2 \cos \omega t \quad m_1 e\omega^2 \sin \omega t \quad 0 \quad 0 \quad F_{ERx} \quad F_{ERy}]^{\mathrm{T}}.$$

Assume that the moving part of the ER damper, together with the outer ring of the bearing B, undergoes translation with velocity $V_B(t)$

$$V_B(t) = (\dot{x}_B^2 + \dot{y}_B^2)^{1/2}. \tag{4}$$

The velocity vector forms an angle δ with the axis x, and

$$\tan \delta = \dot{y}_B / \dot{x}_B. \tag{5}$$

The 1 # ER fluid used in the analysis can be modeled as a Bingham fluid under the electric field [7]. The shear stress τ_z is

$$\tau_z = \tau_d + \eta\dot{\gamma} \tag{6}$$

where η is the viscosity of the ER fluid and $\dot{\gamma}$ is the shear rate, which has $\dot{\gamma} = V_B(t)/c$ in this model, c is the gap between two shear disks.

The yield stress τ_d is proportional to E_e^2 [7], such that

$$\tau_d = A_{ER}E_e^2 = A_{ER}(V_e/c)^2 \tag{7}$$

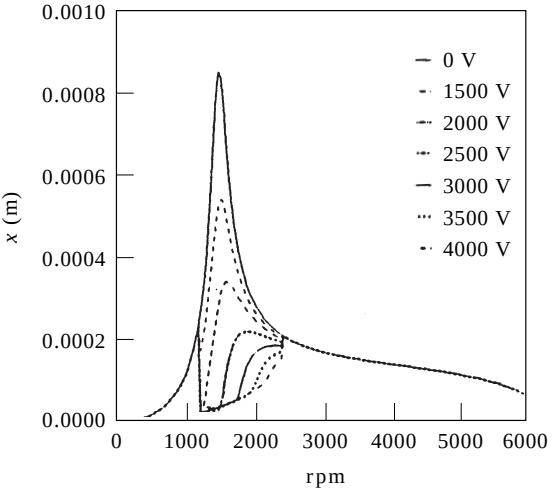

Figure 6. Response curve of B.

where E_e is the electric field strength, V_e is the voltage imposed on two poles, and A_{ER} is a coefficient related to the performance of the ER fluid. Substituting equation (7) into equation (6), we can obtain

$$\tau_z = \eta V_B(t)/c + A_{ER}(V_e/c)^2. \tag{8}$$

Integrating τ_z in the whole shear faces, we obtain the total damping force

$$F_{ERf} = c_{ER} V_B(t) + F_f \tag{9}$$

where c_{ER} is the viscous coefficient

$$c_{ER} = n\pi\eta(R_2^2 - R_1^2)/c. \tag{10}$$

The friction force induced by the imposed electric field is

$$F_f = n\pi(R_2^2 - R_1^2)A_{ER}(V_e/c)^2 \tag{11}$$

where R_2 and R_1 are the outer radius of moving disks and the inner radius of stationary disks, respectively, and n is the number of friction faces. F_f is a Coulomb force which is always opposite to the velocity. The components of F_f in the x and y directions are

$$F_{ERx} = -F_f \cos\delta \qquad F_{ERy} = -F_f \sin\delta. \tag{12}$$

Equation (3) can be solved after substituting equations (10), (11) and (12) in.

4. NUMERICAL SOLUTION

Equation (3) can be expressed as 12 first order differential equations. The fourth order Runge–Kutta method is used to obtain the steady state response of equation (3) for different rotational speeds.

The steady state responses are calculated under different electric fields for rotational speed from 240 to 6000 rpm. The imposed voltages are 0, 1000, 1500, 2000, 2500, 3000 and 3500 V, corresponding to 0, 0·5882, 0·8824, 1·176, 1·47, 1·764

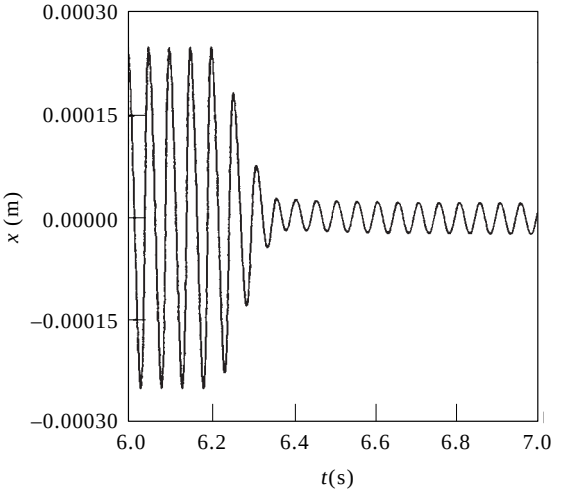

Figure 7. Response of B at speed 1200 rpm imposing 2000 V.

and 2·058 kV/mm in electric field strengths respectively. The responses of bearing B in the x direction versus speed are shown in Figure 4 under different electric fields. Figure 5 shows the orbits of B at critical speed under different electric fields. It can be seen that the larger the strength of the electric field, the smaller the vibration amplitudes at the critical speed.

Though the vibration amplitude can be effectively suppressed by imposing the electric field on the ER damper around the critical speed, the effect of vibration suppression on longer exists when the speed is over 2600 rpm. This might be caused by the Coulomb friction component of the ER damper. To avoid this side-effect, an on/off control is suggested to suppress vibration around the critical speed. Figure 6 shows the response amplitudes versus speed under different electric fields and under the condition that the electric field is imposed at the speed

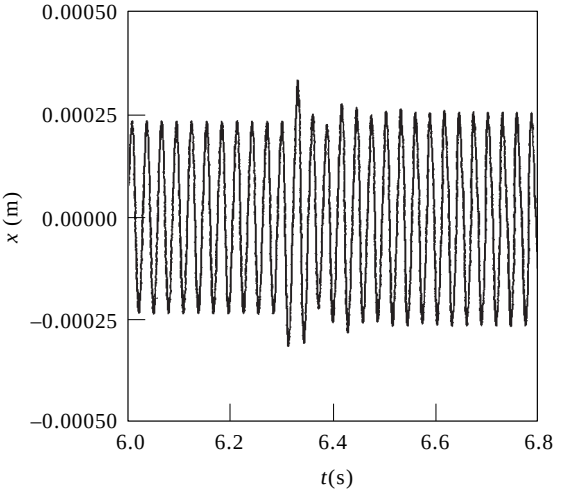

Figure 8. Response of B at speed 2600 rpm when 2000 V is cut off.

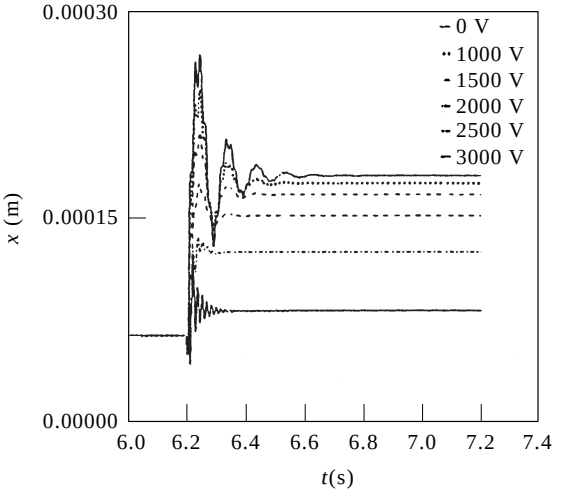

Figure 9. Sudden unbalance response of B via time at speed 2100 rpm.

1200 rpm and is cut off at the speed 2600 rpm. This reveals that the on/off control is very effective in controlling the vibration around the critical speed.

Computations are also carried out to ascertain whether the on/off control method will cause instability to the rotor system. Results are shown in Figures 7 and 8. In the computation, we assume that the electric field reaches its steady state within 0·1 s and the ER fluid will turn from solid-like gel into liquid state immediately when the electric field is cut off. Figure 7 shows the response of B at the speed 1200 rpm when the electric field is switched on, while Figure 8 shows the response B at the speed 2600 rpm when the electric field is cut off. It can be seen that the response of the rotor system reaches a new steady state very quickly, so that the switching on and off of the electric field does not cause instability to the rotor system.

5. SUDDEN UNBALANCE RESPONSE

A sudden unbalance force, e.g., a blade loss, will cause large instantaneous vibration to the rotor system, which may destroy the rotor system itself. The traditional control takes a much longer response time compared with the time of the sudden unbalance process. ER fluid has the merit that it takes a much shorter time to respond to the imposed electric field, so that it is very suitable for

TABLE 1

Instantaneous peak values (theoretical results)

Strengths (kV/mm)	0	0·588	0·882	1·18	1·47	1·76
Peak values (mm)	0·27	0·23	0·20	0·17	0·13	0·12

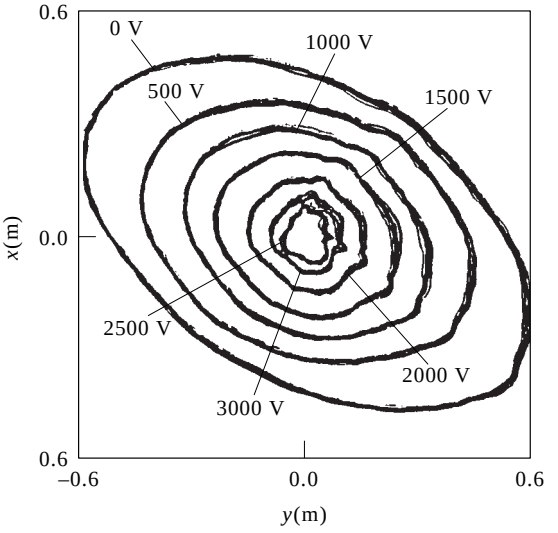

Figure 10. Critical orbits of D under different electric fields (experiment).

controlling the vibration caused by the sudden unbalance force. Generally, a sudden unbalance force can be described analytically as [8]

$$\beta_{[r,s]}(t) = \int_{-\infty}^{t} \bar{\alpha}_{[r,s]}(t)\,\mathrm{d}t \Big/ \int_{-\infty}^{\infty} \bar{\alpha}_{[r,s]}(t)\,\mathrm{d}t \tag{13}$$

where

$$\bar{\alpha}_{[r,s]}(t) = \begin{cases} \exp(-1/(t-r)(s-t)) & r < t < s \\ 0 & \text{others} \end{cases}. \tag{14}$$

When r approaches s, $\beta_{[r,s]}(t)$ approaches the step function and has

$$\beta_{[r,s]}(t) = \begin{cases} 0 & t \leqslant r \\ 1 & t \geqslant s \end{cases}. \tag{15}$$

Hence, $\beta_{[r,s]}(t)$ not only has the characteristic of a step function, but also keeps the transition smooth enough, which makes it very suitable for describing the sudden unbalance force.

The amplitude of unbalance force in equation (1) or equation (3) can be expressed as:

$$u_s = m_1 e\omega^2 + m_2 e\omega^2 \beta_{[r,s]}(t) \tag{16}$$

and

$$u_s = \begin{cases} m_1 e\omega^2 & t \leqslant r \\ m_1 e\omega^2 + m_2 e\omega^2 & t \geqslant s \end{cases} \tag{17}$$

where $m_1 e\omega^2$ is the unbalance element, $m_2 e\omega^2$ is the sudden unbalance element, and r and s are the beginning and end instants of the sudden unbalance process. Substituting equation (17) into equation (3), the governing equations can be expressed as:

$$\mathbf{M\ddot{u}} + \mathbf{C\dot{u}} + \mathbf{Ku} = \mathbf{F} \tag{18}$$

where **M**, **C**, **K** and **u** have the same expressions as those in equation (3), and **F** is expressed as

$$\mathbf{F} = [\{m_1 e\omega^2 + m_2 e\omega^2 \beta_{[r,s]}(t)\} \cos \omega t,$$

$$\{m_1 e\omega^2 + m_2 e\omega^2 \beta_{[r,s]}(t)\} \sin \omega t,\ 0,\ 0,\ F_{ERx},\ F_{ERy}]^{\mathrm{T}}. \tag{19}$$

Assume that the electric field is switched on 0·005 s after the occurrence of the sudden unbalance and the electric field reaches steady state within 0·1 s.

Figure 9 shows the transient responses of B versus time under different electric fields. The instantaneous peak values are shown in Table 1. From these figures and the table, conclusions can be drawn:

(1) The sudden unbalance responses are effectively suppressed by the ER damper. With the increase in the electric field, the instantaneous peak values (the maximum value in transient process is defined as the instantaneous peak value in this paper) of the sudden unbalance decreases.

(2) With the increase in the electric field, the transient process becomes shorter.

(3) With the increase in the electric field, the vibration amplitude of the new steady state decreases.

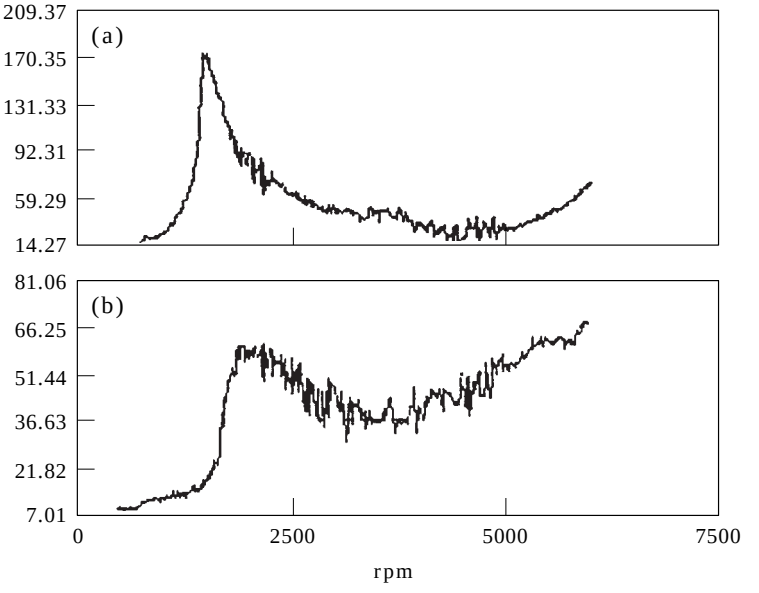

Figure 11. Bode graphs of rotor response in accelerating under different electric fields (experiment). (a) 0 V; (b) 2500 V.

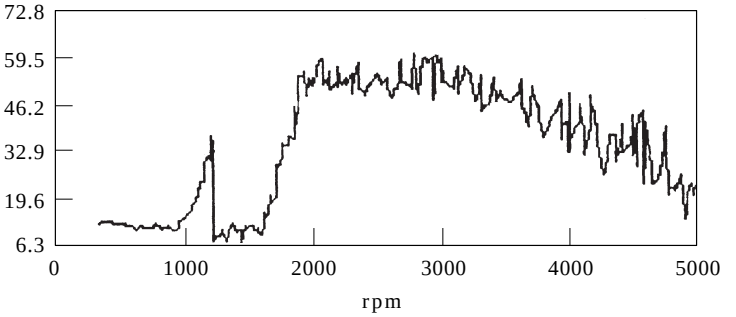

Figure 12. Bode graphs of rotor response in accelerating with 3000 V imposing on at speed 1200 rpm and cutting off at speed 2600 rpm (experiment).

The ER damper is very effective for suppressing the sudden unbalance response and the vibration around the critical speed. When a sudden unbalance occurs at the speed greater than the first critical speed, the ER damper can not only suppress the sudden unbalance, but also suppress the vibration when the rotor is decelerated across the first critical speed.

6. EXPERIMENTAL RESULTS

The experimental rig is shown in Figure 2. Two electric eddy current transducers are fixed at the disk D in horizontal and vertical directions to measure displacements in the x and y directions.

The d.c. signal is filtered out before the signals are input to the oscilloscope to monitor the critical orbit and recorded on the TAEC SR50 recorder. Another electric eddy current transducer is used for measuring the rotational speed.

Recorded signals are sampled by an AD/DA adapter, then processed by a computer to obtain the orbits and the responses. The waterfall graphs are obtained

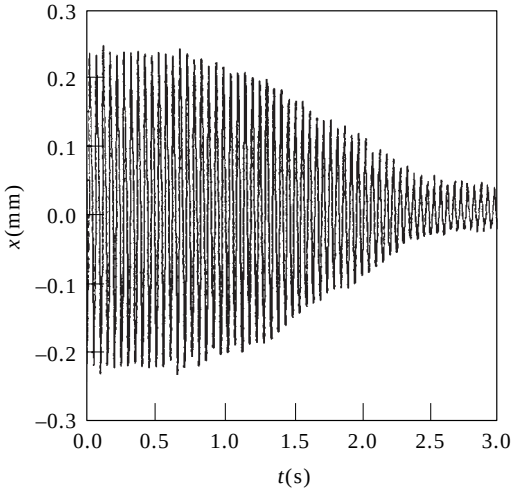

Figure 13. Response of rotor with 3000 V imposing on at speed 2100 rpm (experiment).

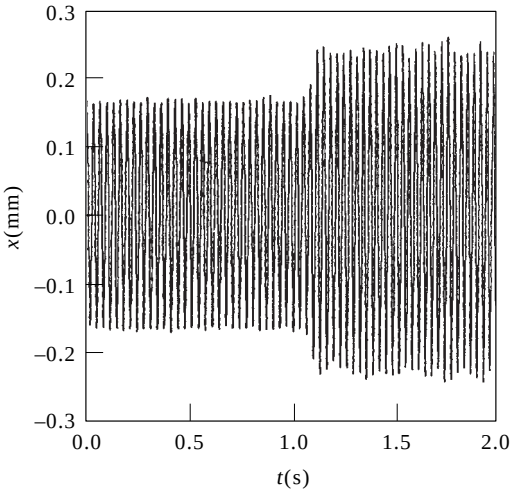

Figure 14. Response of rotor with 2000 V cutting off at speed 2100 rpm (experiment).

by the SA 390 and the Bode graphs are obtained by the DCAM-6000, both directly from the recorded signals. The critical orbits under different electric fields are shown in Figure 10. The critical amplitude decreases sharply as the electric field increases. The Bode graphs are shown in Figure 11. Because the signals are not pre-processed, these graphs are not so smooth when the rotational speed is higher than the critical speed. The first critical resonance is suppressed by the ER damper, and as the electric field increases, the first critical speed shifts to a higher value, which is due to the ER damper having the capability to change the stiffness as well. The Bode graphs with the on/off control are shown in Figure 12. The vibration amplitude around the critical speed was suppressed effectively. Figures 13 and 14 show the responses when an electric field is imposed at the speed 1200 rpm and is then cut off at the speed 2400 rpm, respectively. The rotor system jumps from a steady state to a new steady state without causing instability. The transient process is very short and the instantaneous peak values lie in the permissive range. Figure 15 shows the waterfall graphs of the rotor response in an accelerating process. The first resonant responses are predominant and the amplitude around the critical speed decreases as the electric field increases, which are in accordance with the Bode graphs.

The sudden unbalance experiments are done for voltages 0, 1000, 1500, 2000, 2500 and 3000 V. The electric field is imposed while the balance weight is knocked off. Table 2 shows the instantaneous values under different electric fields. The instantaneous value decreases as the electric field strength increases. The sudden unbalance response is suppressed successfully by the ER damper.

7. CONCLUSIONS

Conclusions can be drawn from theoretical and experimental analysis of the rotor system with the ER damper:

(1) The ER damper can suppress large vibration amplitudes around the critical speed. The ER damper has the capabilities to change both the damping and the stiffness under the electric field.

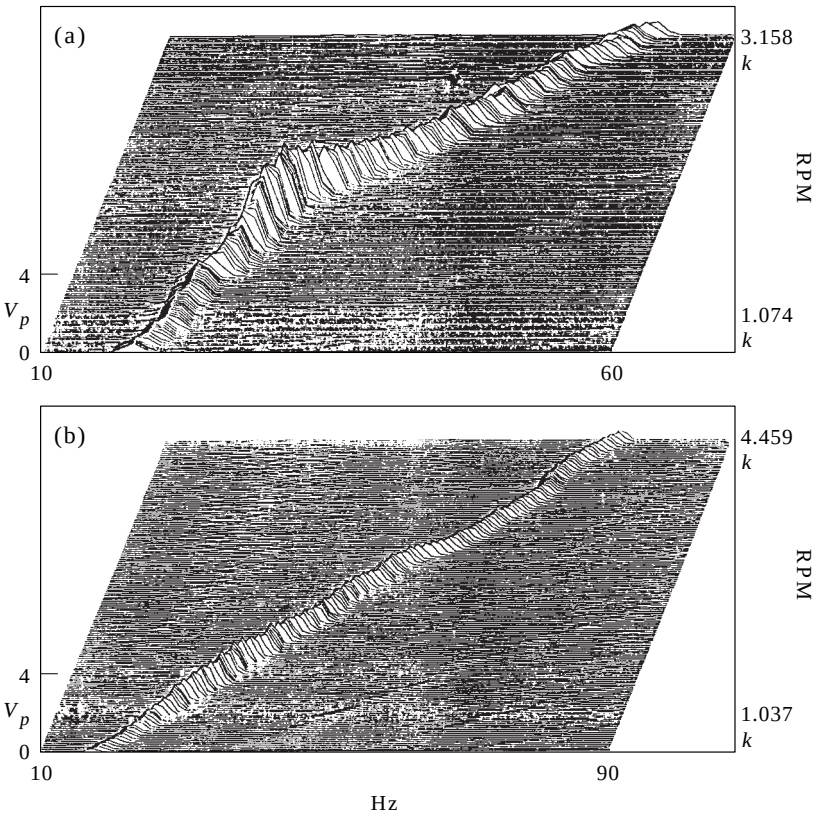

Figure 15. Waterfall graphs of rotor response in accelerating under different electric fields (experiment). (a) 0 V; (b) 2000 V.

TABLE 2

Instantaneous peak values (*experimental results*)

Strengths (kV/mm)	0	0·588	0·882	1·18	1·47	1·76
Peak values (mm)	0·169	0·109	0·088	0·081	0·078	0·075

(2) The on/off control can suppress resonance successfully and will not cause instability to the rotor system.

(3) The ER damper can suppress the sudden unbalance response, shorten the transient process and reduce the amplitude of the new steady state.

(4) The analytical model is very effective in analyzing the steady responses and the sudden unbalance responses. Theoretical results agree with the experimental results to a great extent.

ACKNOWLEDGMENTS

The financial supports from the Natural Science Foundation of China and the Foundation of the State Key Laboratory of Mechanical Structural Strength and Vibration in Xi'an Jiao Tong University are appreciated. Help from M. Xu, Z. C. Yang and M. F. Liao is appreciated.

REFERENCES

1. W. M. WINSLOW 1947 *US Patent* 2,147,750. Methods and means of translating electrical impulses into mechanical force.
2. G. Z. YAO, G. MENG and T. FANG 1995 *Journal of Machine Vibration* **4**, 232–240. The characteristics of electrorheological fluid and its application for vibration control.
3. J. L. NIKOLAJSEN and M. S. HOQUE 1990 *Journal of Vibration and Acoustics*, *Trans. ASME* **112**, 440–443. An electroviscous damper for rotor applications.
4. A. KOLLIAS and A. D. DIMAROGONAS 1993 *Third International Conference on Adaptive Structures*. Technomic, 176–193. Damping of rotor vibration using electro-rheological fluids in disc type devices.
5. G. MENG, D. Z. YING and G. Z. YAO 1996 *Journal of Aerospace Power* **11**, 265–268. Experimental investigation on rotor vibration control by electrorheological damper (in Chinese).
6. J. L. GU *et al*. 1985 *Rotordynamics*. Beijing: Defense Industry Publisher (in Chinese).
7. G. Z. YAO 1997 *Ph.D. dissertation*, *Northwestern Polytechnical University*. Electrorheological fluid and its applications to vibration control (in Chinese).
8. G. MENG 1988 *Ph.D. dissertation*, *Northwestern Polytechnical University*. Study on nonlinear characteristics of flexible rotor-SFD system (in Chinese).